Remote Hydrogen Plasma Chemical Vapor Deposition of Silicon–Carbon Thin-Film Materials from a Hexamethyldisilane Source: Characterization of the Process and the Deposits

A. M. Wróbel,[1] A. Walkiewicz-Pietrzykowska,[1] J. E. Klemberg-Sapieha,[2] Y. Hatanaka,[3] T. Aoki,[3] Y. Nakanishi[3]

[1]*Centre of Molecular and Macromolecular Studies, Polish Academy of Sciences, Sienkiewicza 112, PL-90-363 Łódź, Poland*
[2]*Groupe des Couches Minces and Department of Engineering Physics and Materials Engineering, Ecole Polytechnique, Montreal, Quebec H3C 3A7, Canada*
[3]*Research Institute of Electronics, Shizuoka University, Hamamatsu 432, Japan*

Received 25 April 2001; accepted 7 February 2002

ABSTRACT: Amorphous, hydrogenated silicon–carbon (a-Si:C:H) films were produced by remote hydrogen plasma chemical vapor deposition (RHP-CVD) with hexamethyldisilane (HMDS) as the starting compound. Microwave hydrogen plasma was the source of the atomic hydrogen active species. The susceptibility of particular bonds in the HMDS molecule toward the initiation step was established with tetramethylsilane as a model compound. The reaction mechanisms proposed for the RHP-CVD process revealed the important role of polymerization in film growth. The temperature dependence of the film growth rate implied that the investigated RHP-CVD was a nonthermally activated process. The a-Si:C:H films produced at different deposition temperatures were characterized in terms of their chemical structure, surface and bulk composition, surface morphology, surface free energy, density, corrosion resistance, mechanical properties (adhesion and hardness), and optical properties (refractive index and optical band gap). The deposition temperature appeared to be a key parameter, precisely controlling the structure and properties of the resulting films. Based on the results of these studies, reasonable structure–property relationships were found. © 2002 Wiley Periodicals, Inc. J Appl Polym Sci 86: 1445–1458, 2002

Key words: cold plasma; films; structure

INTRODUCTION

Remote plasma chemical vapor deposition (CVD), also termed *indirect* or *downstream plasma chemical vapor deposition*, has become in recent years a very important method for the fabrication of defect-free, high-quality thin-film materials for advanced technology.[1,2] This technique substantially differs from conventional direct plasma chemical vapor deposition (DP-CVD) in two major aspects. First, the plasma generation and film deposition take place in spatially separated regions. Second, the plasma is induced in a region free of a source compound, unlike DP-CVD, with a simple, non-film-forming gas that is either chemically inert (e.g., argon or helium) or reactive (e.g., hydrogen, oxygen, nitrogen, or ammonia).[1,2] The selected active and electrically neutral species are transported from the plasma region, through the remote section (a trap for electrons, ions, and ultraviolet photons), to the reactor, where they induce the CVD process. Because of these aspects, remote plasma CVD offers well-controlled growth conditions free of film damaging effects, such as charged-particle bombardment or high-energy ultraviolet irradiation, which are inherently involved in DP-CVD.[3]

In this work, we used molecular hydrogen as an upstream gas for plasma generation. In this way, the CVD process was induced with an exclusive contribution of ground-state hydrogen atoms fed to the reactor from the plasma region.[4–7] This allowed us to predict the chemistry of the CVD process, which was determined by the reactivity of the source compound in the atomic hydrogen environment. It is noteworthy that remote hydrogen plasma chemical vapor deposition (RHP-CVD) has been successfully used for the fabrication of a broad class of technologically important thin-film materials, including silicon-based films such as amorphous hydrogenated silicon (a-Si:H),[8–13] silicon carbide (a-Si:C:H),[5,14–20] silicon nitride (a-Si:N:H),[21,22] and silicon carbonitride (a-Si:N:C:H)[23] and

Correspondence to: A. M. Wróbel (amwrobel@bilbo.cbmm.lodz.pl).

Contract grant sponsor: KBN; contract grant number: 7T08C03118.

© 2002 Wiley Periodicals, Inc.

metal-based films such as Zn:S:Se,[24] Ga:As,[25] Cu,[26] Ti:N,[27] and Ta:N.[28]

Taking into account the results of our earlier study,[6,7] which determined the susceptibility of a number of alkylsilanes and alkylcarbosilanes to the RHP-CVD process, we selected hexamethyldisilane [HMDS; $(Me_3Si)_2$] as a very effective source compound for the production of the a-Si:C:H films. In view of our most recent studies,[29] HMDS forms films suitable for the surface modification of polymer materials. Polycarbonate and polypropylene coated with HMDS films revealed marked surface hardening and improved resistance to degradation by ultraviolet irradiation.[29] This article characterizes the chemistry and kinetics of the RHP-CVD process, as well as the resulting a-Si:C:H thin-film materials, in terms of the effect of the deposition temperature on the film structure, composition, surface morphology, and properties important for practical applications.

EXPERIMENTAL

Remote plasma CVD system

The remote plasma CVD system used for the production of the a-Si:C:H films, similar to that described earlier,[6] is schematically shown in Figure 1. The apparatus consisted of three major parts: a plasma generation section (made from a Pyrex glass tube with a 28-mm i.d.) coupled via a resonant cavity and a wave guide with a 2.45-GHz microwave power supply unit; a remote section equipped with a Wood's horn photon trap; and a CVD reactor (made from Pyrex glass by HWS, Mainz, Germany) containing greaseless conical joints, 20-cm-diameter flat flanges sealed with an O-ring, and a stainless steel 13-cm-diameter substrate holder equipped with a heater. A source compound injector (4-mm i.d.) was located approximately 4 cm in front of the substrate holder. Deposition experiments were performed at a total pressure of $p = 0.56$ Torr (75 Pa), a hydrogen flow rate of $F(H_2) = 100$ sccm, a microwave power input of $P = 150$ W, and a substrate temperature of $T_S = 30-400$°C. The HMDS source compound was fed into the CVD reactor at an evaporation temperature of 25°C at a flow (or feeding) rate of F(HMDS) = 3.6 mg min^{-1} = 0.6 sccm. The flow rate of hydrogen was controlled with an MKS (Andover, MA) mass-flow controller. For the source compounds, a mass-flow controller was used to maintain a constant flow, and the flow rate was estimated gravimetrically. Films were deposited on Fisher microscope coverglass plates (50 mm × 45 mm × 0.2 mm) for kinetic measurements, on p-type c-Si wafers for spectroscopic analyses, on Asahi Glass quartz plates (18 mm × 18 mm × 0.5 mm) for optical absorption and scratch-adhesion measurements, and on polished carbon steel plates for corrosion tests. The distance between the plasma edge and the source compound inlet was 30 cm. No deposition was observed in the plasma region; this indicated that there was no back diffusion of a source compound.

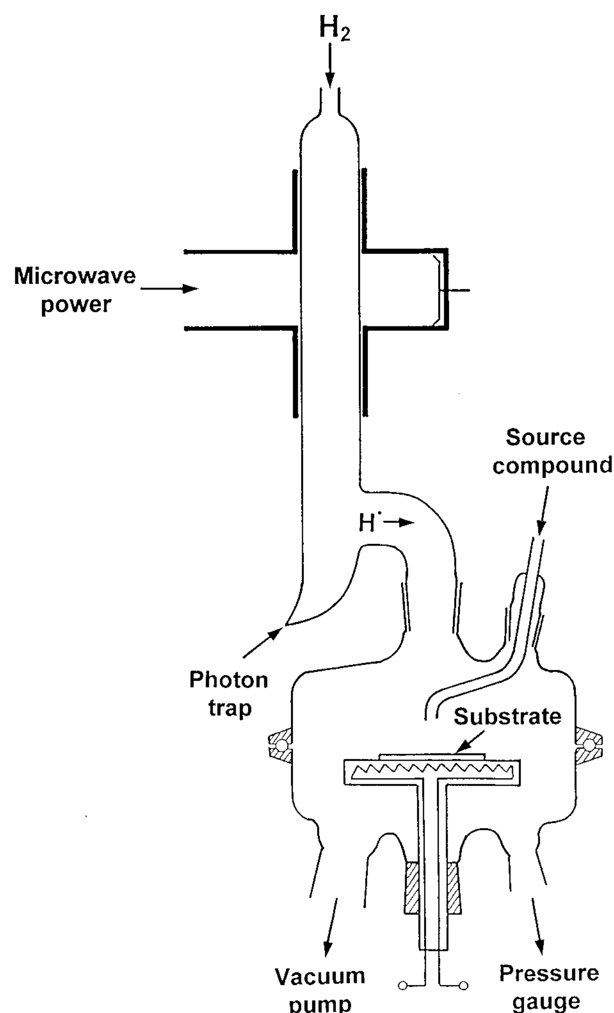

Figure 1 Scheme of the remote plasma CVD apparatus used for film deposition.

Ellipsometric measurements

The thicknesses and refractive indices of the films deposited on c-Si wafers were measured ellipsometrically with a Nippon Infrared Industrial Co. EL-101D (Tokyo) ellipsometer equipped with a 632.8-nm He–Ne laser.

Spectroscopic measurements

Fourier transform infrared (FTIR) absorption spectra of the HMDS source compound and the a-Si:C:H films, deposited on p-type c-Si wafers, were recorded in the transmission mode on an Infinity ATI Matson (Madison, WI) FTIR spectrophotometer. The spectrum of the HMDS liquid source compound was recorded

for a liquid film about 0.1 mm thick. Deconvolution of the FTIR absorption envelopes into individual absorption bands was performed with Gaussian functions for curve fitting.

X-ray photoelectron spectroscopy (XPS) of the films was run on a VG-ESCALAB 3 Mark II (VG Scientific Industrial Estate, Sussex, UK) surface analytical instrument with Mg Kα X-rays as the photoexcitation source with an electron takeoff angle of 45° from the surface normal. Before the XPS analysis, the surface of the film sample was cleaned by sputter-etching with a 1-kV Ar^+ beam.

Auger electron spectroscopy (AES) analysis was performed with an ULVAC AQM 808 (Chigasaki, Japan) system. For the recording of AES spectra for the bulk region (at a depth of ca. 100 nm), the films were subjected to sputter-etching with a 2-kV Ar^+ beam before the AES analysis. The atomic composition of the films was determined from the intensity of doubly integrated AES bands with the sensitivity factors 0.35, 0.18, and 0.50 for Si, C, and O, respectively.

Optical absorption was measured in the range of 190–820 nm for the film samples deposited on quartz plates with a Hewlett–Packard 8452 A (Waldbronn, Germany) ultraviolet–visible spectrophotometer. For the determination of the optical gap, the absorption data were evaluated according to the optical absorption theory for amorphous solids developed by Tauc.[30]

Morphological examination

The surface morphology of the films deposited on the c-Si substrate was examined by scanning electron microscopy (SEM) with a JEOL JSM 6100 (Tokyo) electron microscope and atomic force microscopy (AFM) with a TopoMetrix TMX 2010 (Santa Clara, CA) instrument. AFM examinations were performed at room temperature in air.

Contact-angle measurements

The contact angle was measured at room temperature with a Rame–Hart (Mountain Lakes, NY) goniometer with two test liquids, water and diiodomethane. For each liquid, an average of 5–10 readings was calculated. The contact-angle data were then evaluated for the determination of the dispersion and polar components of the surface free energy according to a model for low-energy surfaces developed by Owens and Wendt.[31]

Scratch-adhesion tests

Mechanical characteristics of the films deposited on quartz substrate were determined with a CSEM (Neuchatel, Switzerland) scratch-adhesion test instrument equipped with a hemispherical Rockwell C diamond indenter with a 200-μm tip radius. The tests were performed with the load increasing linearly at a rate of 1 N min^{-1} and with the tip moving at a speed of 1 cm min^{-1}. The critical load at which the first failure occurred was determined from monitoring of the tangential force, from the acoustic signal emitted during the scratching, or from optical microscopy observations also revealing the failure mode.

TABLE I
Major Neutral Active Species Generated in Hydrogen Plasma (Refs. [32,33])

Neutral active species	Metastable energy (eV)	Radiative lifetime (s)
$H_2(C^3\Pi_u)$	11.75	10^{-4}–10^{-3}
$H(^2S)$	0	—
$H[(2p)^2P^o]$	10.20	1.6×10^{-9}
$H[(3p)^2P^o]$	12.09	5.5×10^{-9}

Corrosion resistance tests

Carbon steel plates coated with the films were immersed in a 5% NaCl water solution at room temperature and brought back into air at a rate of 19 cycles per minute. The delay time recorded for the appearance of rust spots determined the corrosion resistance of the film-coated carbon steel samples.

Materials

The HMDS source compound (Hüls, Piscataway, NJ; 98% purity) was purified by vacuum distillation. The hydrogen upstream gas was 99.99% pure.

RESULTS AND DISCUSSION

Reaction system

In this study, we used low-pressure plasma of hydrogen as the effective source of hydrogen atoms. Because charged species and ultraviolet photons are eliminated from the reaction zone by the remote section equipped with a photon trap (Fig. 1), the neutral active species important for the investigated CVD process have to be considered. Characteristics of the molecular and atomic active neutral species generated in the hydrogen plasma [32,33] are shown in Table I. The contribution of electronically excited and short radiative lifetime species, $H_2(C^3\Pi_u)$, $H[(2p)^2P^o]$, and $H[(3p)^2P^o]$, to RHP-CVD is negligible at a relatively long distance (0.3 m) from the plasma. Therefore, we assume that the ground-state atoms $H(^2S)$ play a major role in the initiation step.

The concentration of the atomic hydrogen in the CVD reactor was determined by the NO_2 titration

method involving the injection of NO_2 into the downstream, which is based on the monitoring of the extinction of characteristic $NO_2\cdot$ chemiluminescence radiation.[6] The determined concentration of atomic hydrogen in the reactor was [H] = 5×10^{15} cm^{-3}, and its feeding rate was F(H) = 27 sccm.[6] Using the last value and the flow rate of the source compound, F(HMDS) = 0.7 sccm, we evaluated the approximate number of hydrogen atoms (N_H) per single molecule of the source compound as $N_H = F(\mathrm{H})/F(\mathrm{HMDS}) \approx 40$ atom/molecule. This accounts for the significantly lower population of active species in RHP-CVD in comparison with DP-CVD.

Chemistry of film formation

Precursor formation step

To obtain information on the reactivity of particular bonds in the molecule of HMDS in the investigated RHP-CVD, we performed the deposition experiments with tetramethylsilane (TMS). The inability to form films found for TMS indicates that the C—H and Si—C bonds are nonreactive in the initiation step. It is interesting to note that TMS readily forms films in DP-CVD.[34–36] This reflects a substantial difference in the mechanisms of DP-CVD and RHP-CVD. The capability of HMDS for film formation is evidently due to the strong reactivity of the Si—Si bonds in the atomic hydrogen environment. The reaction involving an attack of the hydrogen atom on the silicon in the HMDS molecule can be described by eq. (1):

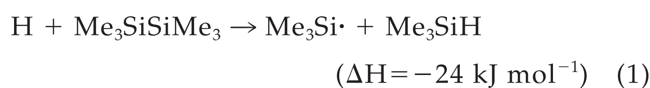

$$\mathrm{H + Me_3SiSiMe_3 \rightarrow Me_3Si\cdot + Me_3SiH} \quad (\Delta H = -24\ \mathrm{kJ\ mol^{-1}}) \quad (1)$$

Trimethylsilyl radicals formed via eq. (1) may undergo either recombination or disproportionation reactions:[37,38]

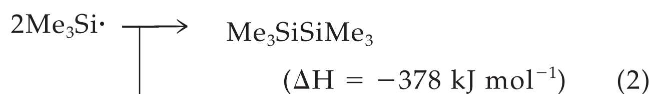

$$\mathrm{2Me_3Si\cdot \rightarrow Me_3SiSiMe_3} \quad (\Delta H = -378\ \mathrm{kJ\ mol^{-1}}) \quad (2)$$

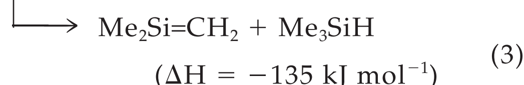

$$\mathrm{2Me_3Si\cdot \rightarrow Me_2Si{=}CH_2 + Me_3SiH} \quad (\Delta H = -135\ \mathrm{kJ\ mol^{-1}}) \quad (3)$$

A secondary reaction of trimethylsilyl radicals with the HMDS source compound may occur:

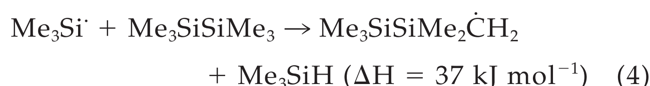

$$\mathrm{Me_3Si^{\cdot} + Me_3SiSiMe_3 \rightarrow Me_3SiSiMe_2\dot{C}H_2 + Me_3SiH} \quad (\Delta H = 37\ \mathrm{kJ\ mol^{-1}}) \quad (4)$$

The radical product of eq. (4) may isomerize and subsequently dissociate:[39,40]

$$\mathrm{Me_3SiSiMe_2\dot{C}H_2 \rightarrow Me_3SiCH_2\dot{S}iMe_2} \quad (\Delta H = -22\ \mathrm{kJ\ mol^{-1}}) \quad (5)$$

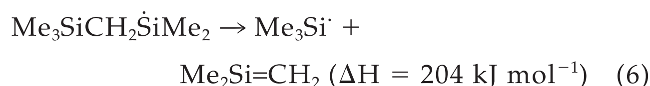

$$\mathrm{Me_3SiCH_2\dot{S}iMe_2 \rightarrow Me_3Si^{\cdot} + Me_2Si{=}CH_2} \quad (\Delta H = 204\ \mathrm{kJ\ mol^{-1}}) \quad (6)$$

The reactions described by eqs. (4) and (6) are endothermic and may, therefore, easily proceed on a heated substrate.

The presented reactions are consistent with the results of our earlier high-resolution gas chromatography/mass spectrometry (GC/MS) examination of the gas-phase conversion products of HMDS formed during RHP-CVD.[7] The GC/MS data revealed that trimethylsilane (Me_3SiH), formed via eqs. (1), (3), and (4), was the major conversion product of HMDS. Moreover, the presence of 1,1,3,3-tetramethyl-1,3-disilacyclobutane [$(Me_2SiCH_2)_2$] found in the conversion products of HMDS is indicative of a head-to-tail dimerization of 1,1-dimethylsilene ($Me_2Si{=}CH_2$),[41,42] formed via eqs. (3) and (6). This compound, a strongly reactive transient intermediate, is considered the major a-Si:C:H film-forming precursor. The heats of the presented reactions were calculated with the thermodynamic data reported by Walsh.[43]

Hypothetical primary steps of film growth

Because of the equivalent biradical and biionic structures ascribed to the silene ⟩Si═C⟨ ↔ ⟩ · Si—C · ⟨ ↔ ⟩$^+$Si—C$^-$⟨),[42,43] units of the 1,1-dimethylsilene precursor formed via the conversion of HMDS have the nature of a classic bifunctional monomer and may contribute to the growth of the a-Si:C:H films via a surface polymerization predominantly involving a polyinsertion mechanism. The growth of the film may take place via a stepwise insertion of the 1,1-dimethylsilene precursor into the Si—Si or Si—C bonds in the HMDS molecules adsorbed on the growth surface. This process propagates linear carbosilane segments [—$(Me_2SiCH_2)_n$—] in the deposit and may be exemplified by eq. (7), which describes schematically a head-to-tail polyinsertion of 1,1-dimethylsilene to the methylsilyl group:

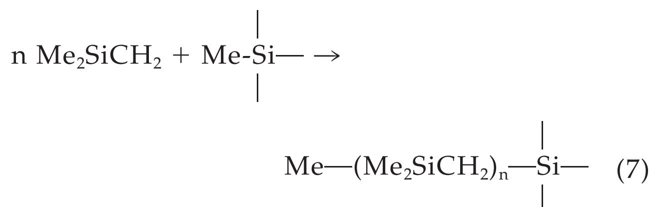

$$\mathrm{n\ Me_2SiCH_2 + Me\text{-}Si\text{—} \rightarrow Me\text{—}(Me_2SiCH_2)_n\text{—}Si\text{—}} \quad (7)$$

Branching of the linear carbosilane segments via an analogous polyinsertion reaction may also take place:

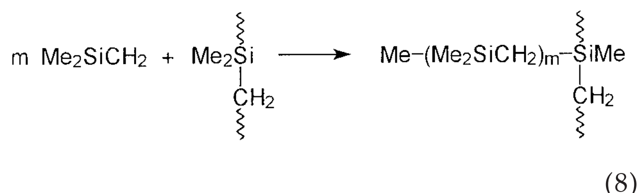

(8)

Reactions described by eqs. (7) and (8) predominate at low T_S values and are consistent with the FTIR structural data discussed in a later section. With increasing T_S, the situation changes dramatically. Because of intense crosslinking, there will be a substantial drop in the carbosilane mer numbers n and m in the linear-branched polycarbosilane structure produced by eqs. (7) and (8). Thermally enhanced surface mobility of adsorbed radicals and vibration of the particular groups in the growing film promote a variety of heterogeneous (gas–solid) and homogeneous (solid–solid) reactions.

The reaction of the atomic hydrogen and trimethylsilyl radicals, formed via eqs. (1) and (6), with the methylsilyl groups in carbosilane segments may result in the abstraction of hydrogen:

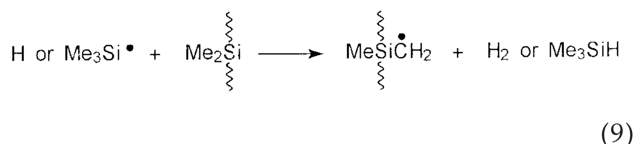

(9)

The radical structure formed in eq. (9) may readily be converted into a silene unit via an endothermic reaction[41,42] involving the elimination of the methyl group:

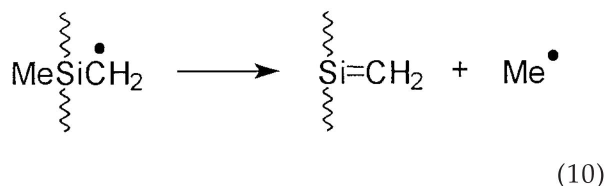

(10)

The methyl radicals effusing from the film may react with methylsilyl groups to produce an intermediate radical structure, as in eq. (9). The reaction described by eq. (10) is particularly important because it involves the elimination of organic moieties from the film. The solid-state-phase reactions of the silene units with the Si—Me groups in the vicinal carbosilane segments of the film (via an insertion mechanism) spontaneously contribute to the first step of crosslinking:

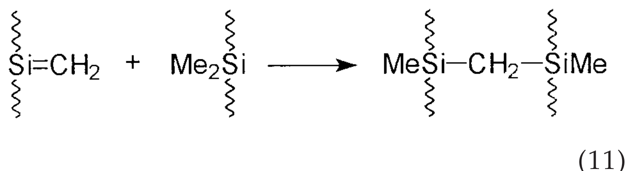

(11)

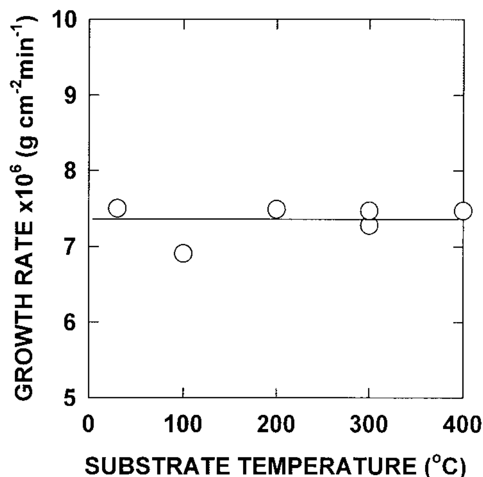

Figure 2 Growth rate of the a-Si:C:H film as a function of T_S.

The dehydrogenation of the carbosilane crosslinks resulting in the formation of carbosilane units with tertiary and quaternary carbon atoms (Si_3CH and Si_4C, respectively) takes place at high deposition temperatures.[17] This process leads to the formation of a three-dimensional Si–carbidic network structure, as confirmed by the FTIR, XPS, and AES observations described in later sections.

Kinetics of film growth and effect of thermal activation

The kinetics of RHP-CVD were investigated by the determination of the deposition time dependencies of the mass and thickness of the films. The linear character of resulting plots accounted for the constant mass- and thickness-based film growth rates. Their values for $T_S = 30°C$ were 75 $\mu g\ cm^{-2}\ min^{-1}$ and 5.2 $nm\ min^{-1}$, respectively.

The effect of thermal activation on the kinetics of RHP-CVD is characterized by the T_S dependence of the film growth rate shown in Figure 2. That there is no effect of T_S on the film growth rate revealed by the data in this figure proves that the examined RHP-CVD is a nonthermally activated process. The rate of surface reactions of film-forming precursors is higher than the rate of their diffusion from the gas phase to the growth surface; therefore, the diffusion seems to be the RHP-CVD rate-limiting factor. A nonthermally activated growth rate of the film also observed for RHP-CVD from disilane[8] and other alkylsilane[4,6,7,19] source compounds seems to be an inherent mechanistic feature of the investigated process. In contrast, the decrease in the film growth rate with rising T_S noted for DP-CVD involving a number of organosilicon sources[44–48] accounts for the adsorption of film-forming precursors on the growth surface as the major growth-rate-limiting factor. This reveals a distinct dif-

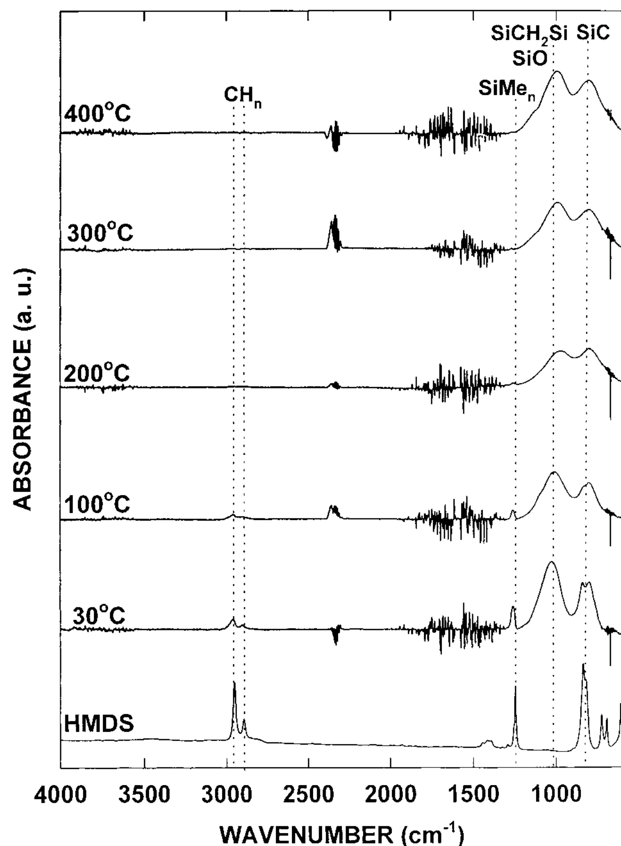

Figure 3 FTIR transmission spectra of a liquid film of an HMDS source compound and a-Si:C:H films deposited on a c-Si substrate heated at T_S = 30, 100, 200, 300, and 400°C.

ference in the mechanisms of both the RHP-CVD and DP-CVD processes.

Film structure

The chemical structure of the a-Si:C:H films deposited at various T_S values is characterized by the FTIR spectra in Figure 3, which shows for comparison the spectrum of the HMDS source compound as well. The assignment of particular absorption bands was based on literature data.[49–52] As can be noted from Figure 4, the film spectra reveal the presence of broad absorption bands with maxima in the range of 1030–1000 and 830–800 cm^{-1} that are characteristic of carbosilane Si—CH_2—Si and carbidic[50–52] Si—C units, respectively. The first band (1030–1000 cm^{-1}) may interfere with the absorption arising from Si—O—Si and/or Si—O—C linkages, which also falls in this region. Weak intensity bands in the range 2960–2900 cm^{-1} are attributed to the C—H stretching mode in CH_n groups (n = 1–3). A low-intensity band at 1260 cm^{-1} originates from the Me deformation mode in the $SiMe_n$ groups(n = 1–3). The increase in T_S involves substantial changes in the film spectra. A significant drop in the intensity of absorption bands from C—H (2960–2900 cm^{-1}) and $SiMe_n$ (1260 cm^{-1}) is due to thermally enhanced scission of the Si—C bonds in the methylsilyl groups. The FTIR data (Fig. 3), indicating an intense cleavage of the Si—Me and Si—Si bonds in the HMDS molecules and the subsequent formation of the chemically more stable carbosilane Si—CH_2—Si units, are consistent with the reactions proposed for the precursor formation and its subsequent polymerization in the film-formation step.

An interesting feature of the film spectra in Figure 3 is the lack of the absorption band near 2100 cm^{-1} from the stretching mode of the Si—H units, which is present in the IR spectra of the HMDS films produced by DP-CVD.[53,54] The formation of the SiH units in the latter process is a fingerprint of the electron-impact fragmentation of the methylsilyl groups.

More precise information on the evolution of the film structure was obtained by the deconvolution of the IR absorption envelopes (ranging from 1300 to 600 cm^{-1}) into the component absorption bands. This is exemplified in Figure 4, which shows deconvoluted FTIR spectra of the films produced at two widely differing T_S values: 30 and 400°C. Both spectra include the component bands from the Si—O (1110–1090

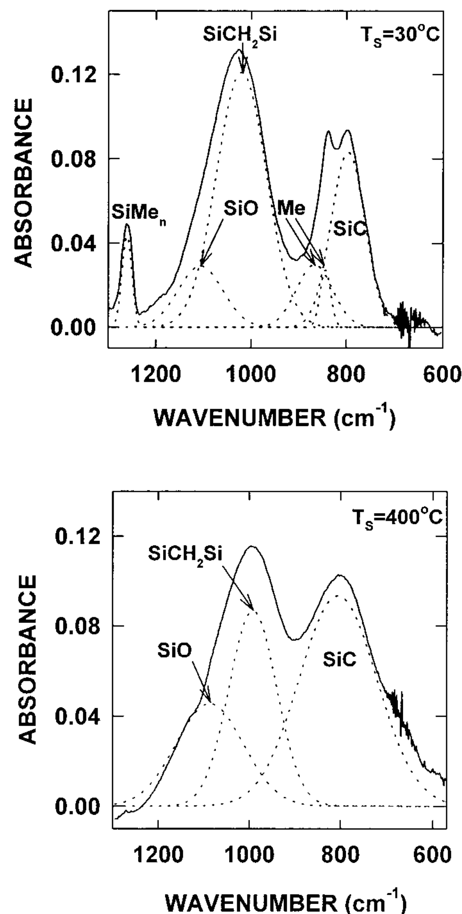

Figure 4 Deconvoluted FTIR spectra of a-Si:C:H films deposited at T_S = 30 and 400°C.

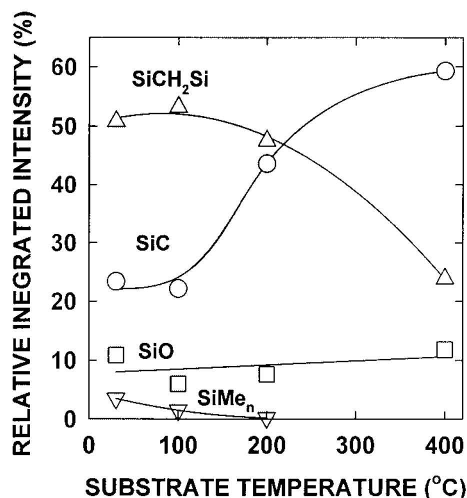

Figure 5 Relative integrated intensity of the FTIR absorption bands from (△) Si—CH_2—Si, (○) Si—C, (□) Si—O, and (▽) $SiMe_n$ units as a function of T_S.

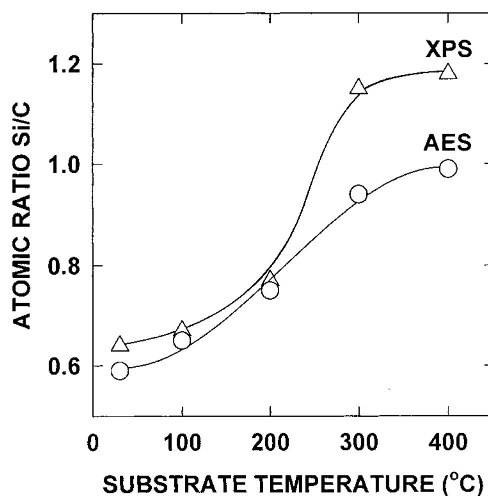

Figure 6 Atomic concentration ratio Si/C as a function of T_S determined for (△) the a-Si:C:H film surface region by XPS and (○) the bulk by AES.

cm^{-1}), Si—CH_2—Si (1020–1000 cm^{-1}), and Si—C (810–800 cm^{-1}) units, and the spectrum for T_S = 30°C also shows the presence of the component bands from the $SiMe_n$ (1260 cm^{-1}) and Me (870 and 840 cm^{-1} from the rocking mode in $SiMe_n$) units. The oxygen contamination revealed by the SiO component band may originate predominantly from the etching of the glass walls of the CVD system with atomic hydrogen during RHP-CVD[17] or from the oxidation of the radical sites in the film after exposure to the atmosphere.

The relative integrated intensities of the component bands ($SiMe_n$, $SiCH_2Si$, SiO, and Si—C), determined as their integrated areas, are shown in Figure 5 as a function of T_S. The decay of the $SiMe_n$ absorption noted in the range T_S = 30–200°C results from the elimination of the methyl groups, as described by eqs. (9) and (10). Moreover, a marked increase in the intensity of the band from the Si—C carbidic units accompanied by the drop in the intensity of the Si—CH_2—Si band is observed with rising T_S. This is associated with thermally enhanced crosslinking, which involves the conversion of the Si—CH_2—Si linkages into carbosilane units with tertiary and quaternary carbon atoms, that is, Si_3CH and Si_4C, respectively.[17] The intensity of the Si—O band is only slightly affected by T_S and remains at a low level.

Film composition

The composition of the Si:C:H films is characterized by the atomic concentration ratio Si/C as the principal stoichiometric parameter. The atomic ratio Si/C determined by XPS for the surface region and by AES for the bulk region as a function of T_S is presented in Figure 6. Si/C for the film surface region and the bulk increases with rising T_S and, at T_S = 400°C, reaches for the bulk (AES data) a value close to unity, which corresponds to that of pure silicon carbide. Very similar values of Si/C for the surface region (XPS data) and bulk (AES data) observed in the low T_S regime 30°C ≤ T_S ≤ 200°C (Fig. 6) account for the good compositional uniformity in the films. Some difference in the values of the XPS and AES ratios that appeared for T_S > 200°C are ascribed to a much higher oxygen content in the film surface region with respect to that in the bulk. Another interesting observation is that the shape of the Si/C plots in Figure 6 is analogous to that of the SiC plot in Figure 5.

Figure 7 shows a correlation between the relative integrated intensity of the IR Si—C band (data from

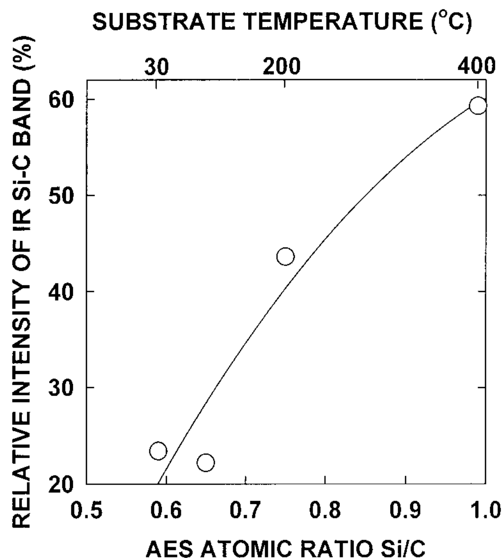

Figure 7 Correlation between the relative integrated intensity of the IR Si—C band (data from Fig. 6) and the AES atomic ratio Si/C controlled by T_S.

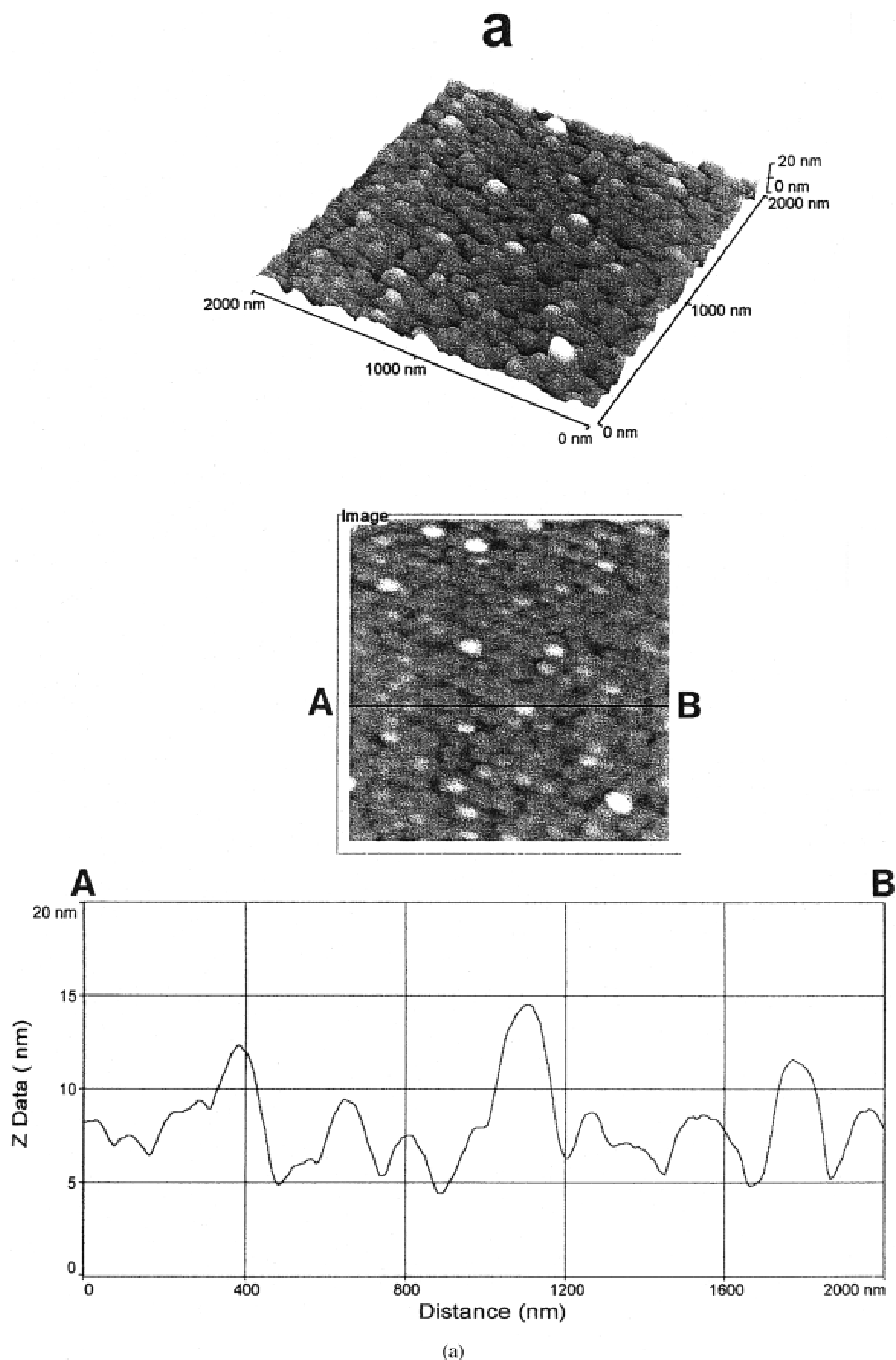

Figure 8 AFM images and cross-sectional surface profiles of a-Si:C:H films deposited at T_S = (a) 30 and (b) 300°C.

Fig. 5) and the AES atomic ratio Si/C controlled by T_S. A drastic increase in the intensity of the Si—C band with Si/C rising again proves the elimination of organic moieties incorporated into the film from the source compound and the formation of the Si–carbidic network in the deposit.

Surface morphology

The results of the SEM study performed for the films produced at five different T_S values (30, 100, 200, 300, and 400°C) indicate that, on the micrometer scale, T_S does not influence the surface morphology of the deposit. The film surface, being very smooth and defect-free, exhibited an excellent morphological homogeneity, regardless of the deposition temperature.

The surface morphology of the examined RHP-CVD films drastically differs from that of the DP-CVD films. The latter materials, in particular those deposited in a low T_S regime, often reveal a morphological heterogeneity manifested by a two-phase structure, which con-

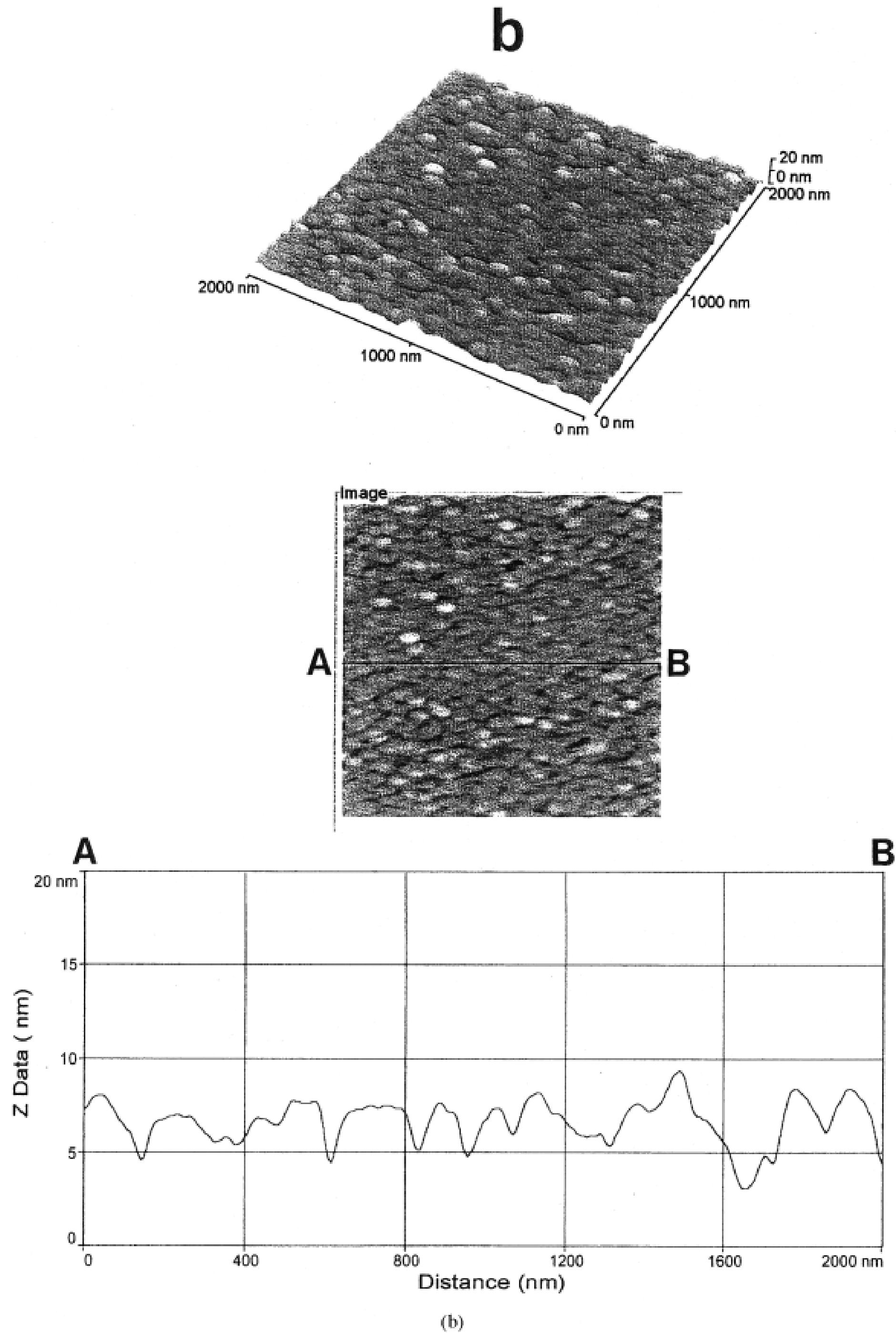

Figure 8 (*Continued from the previous page*)

sists of submicrometer, spheroidal powder particles embedded in a continuous film matrix.[55] According to the literature[55–58] reporting on the surface morphology of the DP-CVD films, the formation of powder particles is associated with the nature of the DP-CVD process and the resulting initiation of the growth step in the gas phase. The coalescence of the particles, which, in turn, start their own growth in the gas phase, is considered to contribute substantially to the film-formation process. The SEM data obtained in this study, in contrast to those of the DP-CVD films,[55–58] suggest a homogeneous mechanism for the growth step in the examined RHP-CVD, which seems to proceed exclusively on the growth surface.

Figure 8 provides AFM images and cross-sectional profiles of the surfaces of RHP-CVD a-Si:C:H films deposited at two different T_S values, 30 and 300°C. In contrast to the SEM data, a distinct effect of this parameter on the film surface morphology is observed on a nanometer scale. As can be noted from Figure 8,

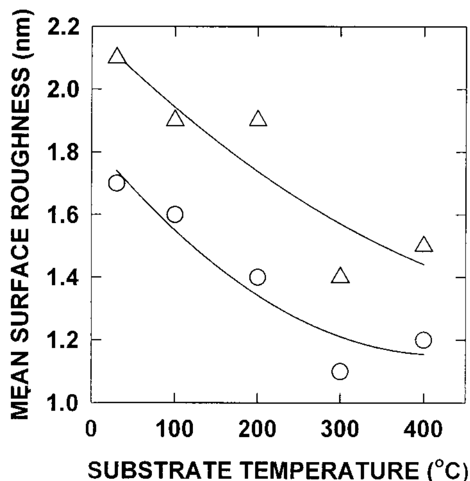

Figure 9 (△) R_{rms} and (○) R_a values of the film surface roughness as a function of T_S.

the increase in T_S from 30 to 300°C involves smoothing of the film surface. This is later illustrated quantitatively in Figure 10, which shows the surface roughness as the arithmetic mean (R_a) and root mean square (R_{rms}) as a function of T_S. The values of the surface roughness drop, R_a from 1.7 to 1.2 nm and R_{rms} from 2.1 to 1.5 nm, with T_S increasing from 30 to 400°C (Fig. 9). This smoothing of the film surface with increasing T_S may be attributed to an enhanced mobility of film-forming precursors at the growth surface and chemical processes resulting in the formation of a highly crosslinked, dense material implied by the observed structural changes.

Film properties

Surface free energy

The surface free energy is a useful parameter that characterizes the physicochemical nature of the film surface and may provide information regarding short-range interaction forces between the film and other material surfaces in a composite system. Figure 10 shows the dispersive component (γ_S^d) and polar component (γ_S^p) of the film surface free energy ($\gamma_S = \gamma_S^d + \gamma_S^p$) as a function of the XPS atomic ratio Si/C (for the surface region) controlled by T_S. In view of the presented surface energy data, γ_S^d varies from 31 to 37 mJ m^{-2} with ratio Si/C or T_S rising, whereas γ_S^p remains almost constant at a relatively small mean value of about 3 mJ m^{-2}. The observed change in γ_S^d can be explained in terms of our earlier findings[59] for the DP-CVD films, which revealed that the dispersive component is sensitive to the crosslink density. Therefore, the increase in γ_S^d with Si/C rising, as follows from Figure 10, is due to the crosslinking process, which causes dense packing of structural elements in the film. The presented data permit us to classify the examined a-Si:C:H films as low-surface-energy and, in particular, low-polarity materials.

Density

The density of the film is presented as a function of the AES atomic ratio Si/C in Figure 11(a) and as a function of the relative intensity of the IR Si—C band (data from Fig. 5) in Figure 11(b). The data points in these figures marked with arrows correspond to the density values calculated from the slopes of the linear plots of the deposition time dependencies of the film mass and thickness, which were specified in an earlier section. A sharp rise in the film density observed with the ratio Si/C [Fig. 11(a)] and the intensity of the Si—C band [Fig. 11(b)] increasing is due to the earlier discussed crosslinking and resulting formation of Si–carbidic networks.

Adhesion and hardness

Film adhesion to the substrate is represented by the critical load (L_C), which was evaluated from the onset of conformal cracks during the scratching procedure. The values of L_C determined for the films differing in thickness were normalized to a thickness of 100 nm, with a linear thickness dependence of L_C assumed.[60,61] Figure 12 shows the plot of a normalized adhesive critical load versus the AES atomic ratio Si/C controlled by T_S. A substantial improvement of the adhesion revealed in Figure 12 by the increase in the normalized critical load with a rising atomic ratio Si/C is attributed to the transformation of the film into a strongly crosslinked and dense material.

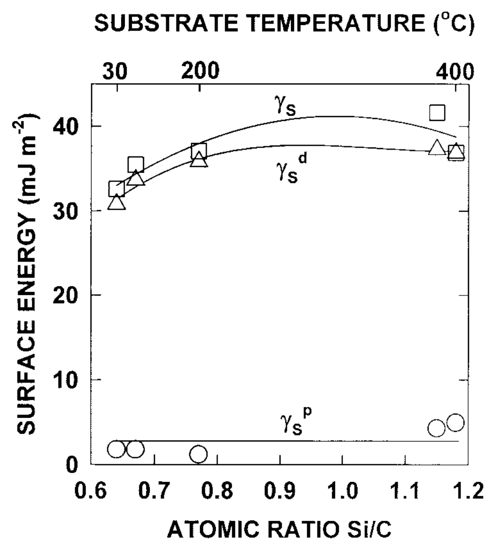

Figure 10 (△) γ_S^d and (○) γ_S^p of (□) γ_S of a-Si:C:H films as a function of the XPS atomic ratio Si/C (for the surface region) controlled by T_S.

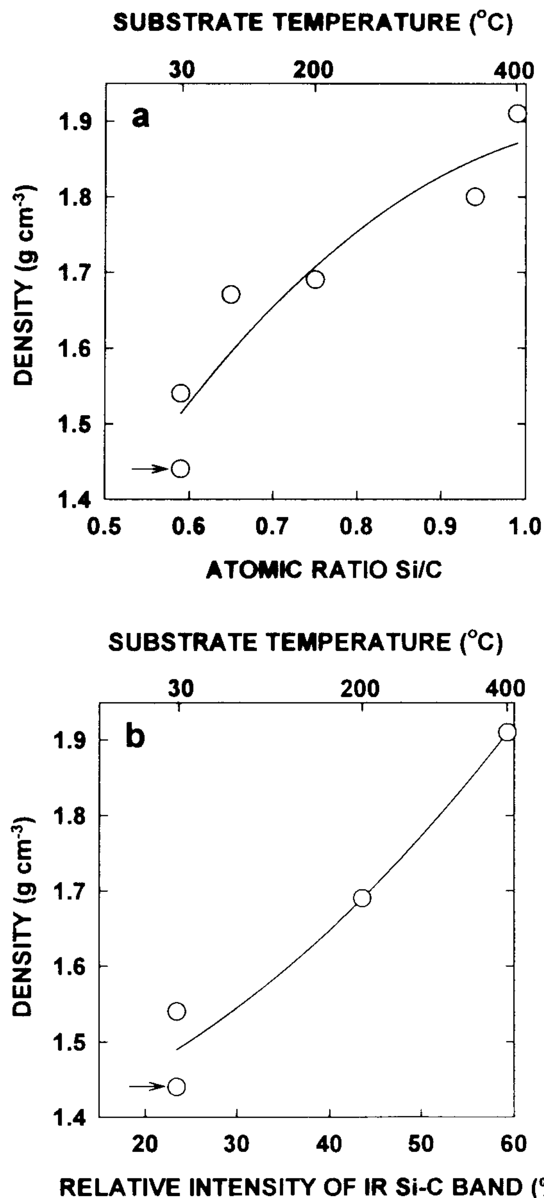

Figure 11 Density of a-Si:C:H films as a function of (a) the AES atomic ratio Si/C and (b) the relative intensity of the IR band Si—C controlled by T_S.

On the basis of the results of scratch-adhesion testing, the scratch hardness (H_S) was estimated from the formula for a hemispherical indenter:[61]

$$H_s = 8L_c/\pi d^2 \qquad (12)$$

Here d denotes the width of the scratch track measured after the test is completed. Figure 13 illustrates the scratch hardness of the a-Si:C:H film as a function of the AES atomic concentration ratio Si/C and/or T_S. The plot in Figure 13 shows that the film hardness drastically increases with the ratio Si/C and/or T_S rising, reaching at T_S = 300–400°C the value H_S = 19–22 GPa. For comparison, the hardness of c-SiC

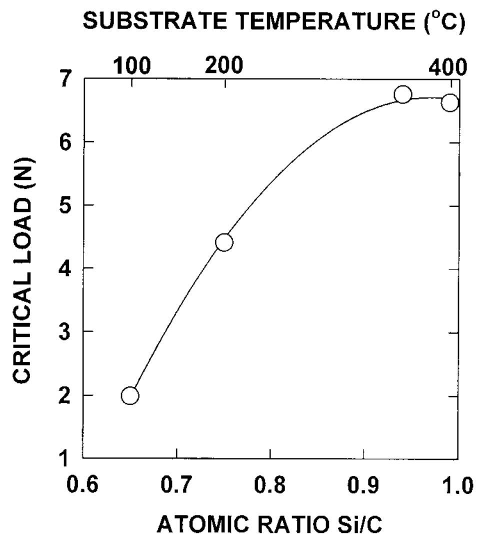

Figure 12 Normalized adhesive critical load for a-Si:C:H films deposited on quartz plates as a function of the AES atomic ratio Si/C controlled by T_S.

(crystalline silicon carbide) is 26 GPa.[62] A marked hardening of the film noted with an increasing atomic ratio Si/C is associated with a thermally enhanced crosslinking process that increases the content of the Si–carbidic structure, as indicated by the increase in the IR absorption from the Si—C carbidic units (Figs. 5 and 7).

Corrosion resistance

Table II summarizes the results of the corrosion resistance test performed for carbon steel plates coated with the a-Si:C:H films produced at various deposition temperatures. The film thickness, density, and stoichiometric parameter Si/C are also specified. The data in

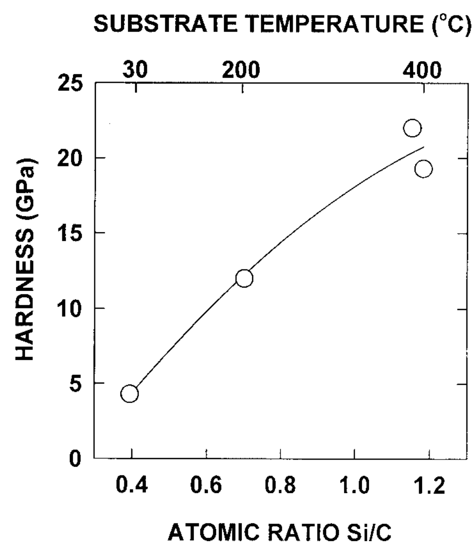

Figure 13 Scratch hardness of a-Si:C:H films as a function of the AES atomic ratio Si/C controlled by T_S.

TABLE II
Corrosion Resistance of a-Si:C:H Film Coated Carbon Steel in 5% NaCl Solution

T_s (°C)	Film thickness (μm)	Film density (g cm^{-3})	AES ratio Si/C	Corrosion delay time (day)
30	2.40	1.53	0.59	8
100	1.40	1.65	0.65	22
300	1.35	1.84	0.94	23

Table II reveal a reasonably good correlation between film the density or parameter Si/C and the corrosion resistance. The delay time to the appearance of corrosion spots increases from 8 to 23 days with the film density and atomic ratio Si/C rising. For an uncoated control steel sample, the corrosion spots appeared after 1 h of testing.

For comparison, a corrosion resistance test performed with a 3.5% NaCl solution as a corrosive medium and carbon steel test samples coated with HMDS films deposited in DP-CVD at a combined energy input to the plasma revealed corrosion delay times ranging from 19 to 23 h.[63]

Refractive index and optical gap

The optical properties of the a-Si:C:H films are characterized by the refractive index (n) and the optical gap (E_o), or absorption edge. Figure 14 shows the variation of n with the AES atomic ratio Si/C controlled by T_S. As follows from the curve in Figure 14, n rises from 1.55 to 1.94 with the atomic ratio Si/C and/or T_S increasing. This trend is presumably due to the densification of the film resulting from thermally enhanced crosslinking, which is reflected by the data

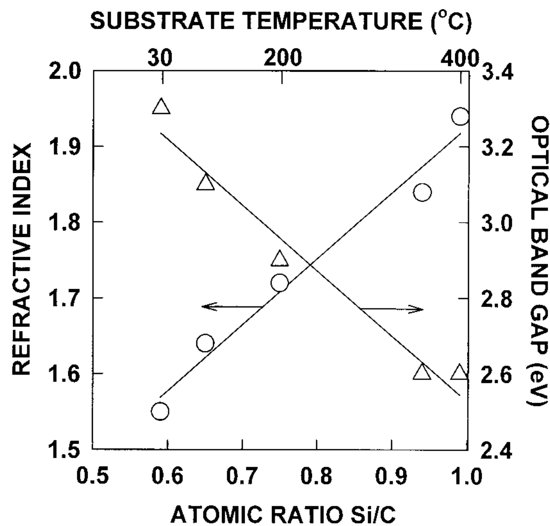

Figure 14 (○) Refractive index at a wavelength of 632.8 nm and (△) optical gap of a-Si:C:H films as a function of the AES atomic ratio Si/C controlled by T_S.

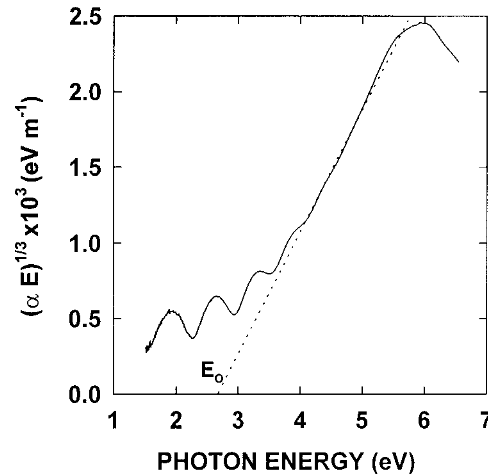

Figure 15 Optical absorption data for a-Si:C:H films produced at T_S = 300°C plotted according to the Tauc expression as $(\alpha E)^{1/3}$ versus E.

in Figure 7. A compositional dependence of n similar to that presented in Figure 14 has also been observed for the a-Si:C:H films produced by RHP-CVD from tetrakis(trimethylsilyl)silane[17] and by DP-CVD from a silane–methane mixture.[64]

E_o was determined by the fitting of the absorption data to the Tauc expression:[30]

$$\alpha E = B(E - E_o)^n \quad (13)$$

where α denotes the absorption coefficient, E is the energy of absorbed photons, B is the dimensionless density-of-states constant, and n is a parameter related to the density-of-states distribution. E_o was determined for n = 3. Figure 15 shows a typical plot of the absorption data evaluated according to the Tauc expression as $(\alpha E)^{1/3}$ versus E. E_o is determined by the extrapolation of a linear portion of the plot to the abscissa axis. Figure 14 shows E_o for the a-Si:C:H film as a function of the atomic ratio Si/C controlled by T_S. E_o decreases linearly from 3.3 to 2.6 eV with Si/C and/or T_S rising. A compositional dependence of E_o similar to that shown in Figure 14 was reported for DP-CVD a-Si:C:H films.[64–66]

The observed compositional and/or deposition temperature dependencies of the optical gap (Fig. 14) may be explained by the formation of localized states and their effect on this quantity. It is expected that dangling bond defects in the film are created during the deposition process, giving rise to the density of the localized states. At low deposition temperatures, the concentration of dangling bonds is low because of their saturation with hydrogen. The concentration of dangling bond defects increases with the deposition temperature because of thermal scission of the C—H and Si—C bonds in the deposit, as proven by the FTIR data in Figures 3 and 5. This involves an extension of

the density-of-states tail and the resulting narrowing of the optical gap.

The presented results indicate that the optical gap width is strongly affected by the film composition and can be precisely controlled by the deposition temperature.

CONCLUSIONS

The investigated RHP-CVD process displays high selectivity with respect to particular bonds in the molecule of the HMDS source compound and is induced with an exclusive contribution of the Si—Si bond, whereas the C—H and Si—C bonds are inactive.

The discussed chemistry, supported by our earlier GC/MS examination of the gas-phase conversion products and this structural study, accounts for the substantial role of polymerization in the formation of the a-Si:C:H thin-film materials from the HMDS source in the RHP-CVD process. The HMDS source compound is converted into 1,1-dimethylsilene ($Me_2Si{=}CH_2$), a transient hot intermediate with the nature of a bifunctional classical monomer, which is assumed to be the major film-forming precursor. Because of a high-reactivity π bond in the silene unit, the precursor may easily undergo surface polymerization via an insertion mechanism, propagating carbosilane [—$(Me_2SiCH_2)_n$—] segments in the deposit. The silene units formed in the deposit by the reaction of the gas-phase radicals with methylsilyl groups in the growing carbosilane segments may contribute to the spontaneous crosslinking via carbosilane Si—CH_2—Si crosslinks.

That there was no observed effect of T_S on the film growth rate proves that the examined RHP-CVD is a nonthermally activated process. The diffusion of film-forming precursors from the gas phase to the growth surface seems to be a growth-rate-limiting factor.

The deposition temperature is a key parameter precisely controlling the structure, composition, and properties of the a-Si:C:H films. The increase in T_S involves the dehydrogenation of the carbosilane Si—CH_2—Si crosslinks in the films, which evolve into Si–carbidic networks, as revealed by the FTIR, XPS, and AES examinations.

The films were found to be low-surface-energy, morphologically homogeneous, powder contamination-free materials with a mean surface roughness of R_a = 1.2–1.7 nm and R_{rms} = 1.5–2.1 nm for T_S = 30–400°C.

The density, adhesion, hardness, and corrosion resistance of the film are strongly influenced by the atomic ratio Si/C and increase markedly with a rising value of this structural parameter.

The refractive index and optical gap of the produced a-Si:C:H films can be controlled by the atomic ratio Si/C over a wide ranges of values; that is, n = 1.55–1.94 and E_o = 2.6–3.3 eV.

In view of the presented properties, the a-Si:C:H films produced by RHP-CVD seem to be very promising coating materials for many applications.

References

1. Lucovsky, G.; Tsu, D. V.; Rudder, R. A.; Markunas, R. J. In Thin Film Processes II; Vossen, J. L.; Kern, W., Eds.; Academic: Boston, 1991; Chapter 4.
2. Luft, W.; Tsuo, W. Y. Hydrogenated Amorphous Silicon Alloy Deposition Process; Marcel Dekker: New York, 1993; Chapter 9.
3. Wróbel, A. M.; Czeremuszkin, G. Thin Solid Films 1992, 216, 203.
4. Wróbel, A. M.; Wickramanayaka, S.; Hatanaka, Y. J Appl Phys 1994, 76, 558.
5. Wróbel, A. M.; Wickramanayaka, S.; Nakanishi, Y.; Hatanaka, Y.; Wysiecki, M. J Chem Vapor Depos 1994, 2, 229.
6. Wróbel, A. M.; Walkiewicz-Pietrzykowska, A.; Stasiak, M.; Aoki, T.; Hatanaka, Y.; Szumilewicz, J. J Electrochem Soc 1998, 145, 1060.
7. Wróbel, A. M.; Walkiewicz-Pietrzykowska, A. Chem Vap Deposition 1998, 4, 133.
8. Yoshida, A.; Inoue, K.; Ohashi, H.; Saito, Y. Appl Phys Lett 1990, 57, 484.
9. Meikle, S.; Nakanishi, Y.; Hatanaka, Y. Jpn J Appl Phys 1990, 29, L2130.
10. Meikle, S.; Nakanishi, Y.; Hatanaka, Y. J Vac Sci Technol A 1991, 9, 1051.
11. Johnson, N. M.; Nebel, C. E.; Santos, P. V.; Jackson, W. B.; Street, R. A.; Stevens, K. S.; Walker, J. Appl Phys Lett 1991, 59, 1443.
12. Kawasaki, M.; Suzuki, H. J Appl Phys 1994, 75, 3456.
13. Kim, D.-H.; Park, Y.-B.; Lee, I.-J.; Rhee, S.-W. J Electrochem Soc 1996, 143, 2640.
14. Yasui, K.; Fujita, A.; Akahane, T. Jpn J Appl Phys 1992, 31, L379.
15. Yasui, K.; Muramoto, M.; Akahane, T. Jpn J Appl Phys 1994, 33, 4395.
16. Wickramanayaka, S.; Hatanaka, Y.; Nakanishi, Y.; Wróbel, A. M. J Electrochem Soc 1994, 141, 2910.
17. Wróbel, A. M.; Wickramanayaka, S.; Nakanishi, Y.; Fukuda, Y.; Hatanaka, Y. Chem Mater 1995, 7, 1403.
18. Wróbel, A. M.; Wickramanayaka, S.; Nakanishi, Y.; Hatanaka, Y. J Mater Process Technol 1995, 53, 477.
19. Wróbel, A. M.; Wickramanayaka, S.; Nakanishi, Y.; Hatanaka, Y.; Pawlowski, S.; Olejniczak, W. Diamond Relat Mater 1997, 6, 1081.
20. Wróbel, A. M.; Wickramanayaka, S.; Kitamura, K.; Nakanishi, Y.; Hatanaka, Y. Chem Vap Deposition 2000, 6, 315.
21. Yasui, K.; Nasu, M.; Komaki, K.; Kaneda, S. Jpn J Appl Phys 1990, 29, 918.
22. Yasui, K.; Nasu, M.; Kaneda, S. Jpn J Appl Phys 1990, 29, 2822.
23. Aoki, T.; Ogishima, T.; Wróbel, A. M.; Nakanishi, Y.; Hatanaka, Y. Vacuum 1998, 51, 747.
24. Fujiwara, H.; Gotoh, J.; Shirai, H.; Shimizu, I. J Appl Phys 1993, 74, 5510.
25. Sato, M. Jpn J Appl Phys 1995, 34, L93.
26. Aoki, T.; Wickramanayaka, S.; Wróbel, A. M.; Nakanishi, Y.; Hatanaka, Y. J Electrochem Soc 1995, 142, 166.
27. Yun, J.-Y.; Rhee, S.-W. Thin Solid Films 1998, 312, 24.
28. Cho, K.-N.; Han, C.-H.; Noh, K.-B.; Oh, J.-E.; Paek, S.-H.; Park, C.-S.; Lee, S.-I.; Lee, M. Y.; Lee, J. G. Jpn J Appl Phys 1998, 37, 6502.
29. Hatanaka, Y.; Sano, K.; Aoki, T.; Wróbel, A. M. Thin Solid Films 2000, 368, 287.
30. Tauc, J. In Optical Properties of Solids; Abeles, F., Ed.; North Holland: Amsterdam, 1972; Chapter 5.
31. Owens, D. K.; Wendt, R. C. J Appl Polym Sci 1969, 13, 1741.

32. Vossen, J. L.; Cuomo, J. J. In Thin Film Processes; Vossen J. L.; Kern, W., Eds.; Academic: New York, 1978; Chapter 2.1, p 46.
33. Okabe, H. Photochemistry of Small Molecules; Wiley-Interscience: New York, 1978.
34. Wróbel, A. M.; Czeremuszkin, G.; Szymanowski, H.; Kowalski, J. Plasma Chem Plasma Process 1990, 11, 277.
35. Wróbel, A. M.; Stańczyk, W. Chem Mater 1994, 6, 1766.
36. Wrobel, A. M.; Walkiewicz-Pietrzykowska, A. J Chem Vapor Depos 1995, 4, 87.
37. Tokach, S. K.; Koob, R. D. J Phys Chem 1979, 83, 774.
38. Tokach, S. K.; Koob, R. D. J Am Chem Soc 1980, 102, 376.
39. Davidson, I. M. T.; Hughes, K. J.; Scampton, R. J. J Organomet Chem 1984, 272, 11.
40. O'Neal, H. E.; Ring, M. A. Organometallics 1988, 7, 1017.
41. Raabe, G.; Michl, J. Chem Rev 1985, 85, 419.
42. Apeloig, Y. In The Chemistry of Organic Silicon Compounds; Patai, S.; Rappoport, Z., Eds.; Wiley: New York, 1989; Chapter 2, p 105.
43. Walsh, R. In The Chemistry of Organic Silicon Compounds; Patai, S.; Rappoport, Z., Eds., Wiley: New York, 1989; Chapter 5, p 371.
44. Secrist, D. R.; Mackenzie, J. D. J Electrochem Soc 1966, 113, 914.
45. Emesh, I. T.; d'Asti, G.; Mercier, J. S.; Leung, P. J Electrochem Soc 1989, 136, 3404.
46. Wrobel, A. M.; Kryszewski, M. Prog Colloid Polym Sci 1991, 85, 91.
47. Favia, P.; Lamendola, R.; d'Agostino, R. Plasma Sources Sci Technol 1992, 1, 59.
48. Niemann, J.; Bauhofer, W. Thin Solid Films 1999, 352, 249.
49. Anderson, D. R. In Analysis of Silicones; Smith, A. L., Ed.; Wiley-Interscience: New York, 1974; Chapter 10.
50. Tsai, H.-K.; Lin, W.-L.; Sah, W. J.; Lee, S.-C. J Appl Phys 1988, 64, 1910.
51. Deplancke, M. P.; Powers, J. M.; Vandentop, G. J.; Salmeron, M.; Somorjai, G. A. J Vac Sci Technol A 1990, 9, 450.
52. Bhusari, D. M.; Kshirsagar, S. T. J Appl Phys 1993, 73, 1743.
53. Wróbel, A. M. J Macromol Sci Chem 1985, 22, 1089.
54. Fonesca, J. L. C.; Tasker, S.; Apperley, D. C.; Badyal, J. P. S. Macromolecules 1996, 29, 1705.
55. Wróbel, A. M.; Wertheimer, M. R. In Plasma Deposition, Treatment, and Etching of Polymers; d'Agostino, R., Ed.; Academic: Boston, 1990; Chapter 3.
56. Boufendi, L.; Bouchoule, A. Plasma Sources Sci Technol 1994, 3, 262.
57. Fridman, A. A.; Boufendi, L.; Hbid, T.; Potapkin, B. V.; Bouchoule, A. J Appl Phys 1996, 79, 1303.
58. Vivet, F.; Bouchoule, A.; Boufendi, L. J Appl Phys 1998, 83, 7474.
59. Wróbel, A. M. In Physicochemical Aspects of Polymer Surfaces; Mittal, K. L., Ed.; Plenum: New York, 1981; p 197.
60. Burnett, P. J.; Rickerby, D. S. Thin Solid Films 1987, 154, 403.
61. Rats, D.; Hajek, V.; Martinu, L. Thin Solid Films 1999, 340, 33.
62. Riedel, R. Adv Mater 1994, 6, 549.
63. Cho, D. L.; Yasuda, H. J Appl Polym Sci Appl Polym Symp 1988, 42, 233.
64. Pascual, E.; Andujar, J. L.; Fernandez, J. L.; Bertran, E. Diamond Relat Mater 1995, 4, 1205.
65. Kuhman, D.; Grammatica, S.; Jansen, F. Thin Solid Films 1989, 177, 253.
66. Pereyra, I.; Carreno, M. N. P.; Tabacniks, M. H.; Prado, R. J.; Fantini, M. C. A. J Appl Phys 1998, 84, 2371.